

Central Lancashire Online Knowledge (CLoK)

Title	Heat Sterilizable Coatings Based on Nafion and Graphene Quantum Dots With Advanced Antibacterial Performance
Type	Article
URL	https://clock.uclan.ac.uk/54169/
DOI	https://doi.org/10.1002/nano.70012
Date	2025
Citation	Beg, Mohammed Suleman, Gibbons, Ella, Duncalf, James, Gavalas, Spyridon, Redman, Daniel, Holden, Mark and Kelarakis, Antonios (2025) Heat Sterilizable Coatings Based on Nafion and Graphene Quantum Dots With Advanced Antibacterial Performance. Nano Select.
Creators	Beg, Mohammed Suleman, Gibbons, Ella, Duncalf, James, Gavalas, Spyridon, Redman, Daniel, Holden, Mark and Kelarakis, Antonios


It is advisable to refer to the publisher's version if you intend to cite from the work.
<https://doi.org/10.1002/nano.70012>

For information about Research at UCLan please go to <http://www.uclan.ac.uk/research/>

All outputs in CLoK are protected by Intellectual Property Rights law, including Copyright law. Copyright, IPR and Moral Rights for the works on this site are retained by the individual authors and/or other copyright owners. Terms and conditions for use of this material are defined in the <http://clock.uclan.ac.uk/policies/>

RESEARCH ARTICLE OPEN ACCESS

Heat Sterilizable Coatings Based on Nafion and Graphene Quantum Dots With Advanced Antibacterial Performance

Mohammed Suleman Beg | Ella Nicole Gibbons | James Duncalf | Spyridon Gavalas | Daniel Redman | Mark A. Holden | Antonios Kelarakis 

UCLan Research Centre for Smart Materials, School of Pharmacy and Biomedical Sciences, University of Central Lancashire, Preston, UK

Correspondence: Antonios Kelarakis (akelarakis@uclan.ac.uk)

Received: 31 December 2024 | **Revised:** 22 February 2025 | **Accepted:** 17 March 2025

Funding: This study was funded by the University Alliance Doctoral Training Alliance under the Marie Skłodowska-Curie COFUND scheme to S.G.; Higher Education Innovation Fund (Research England) and UCLan Research Centre for Smart Materials.

Keywords: antimicrobial | graphene quantum dots | layer-by-layer | Nafion

ABSTRACT

The study focuses on the preparation of electrostatically assembled layer-by-layer waterborne nanocoatings comprising negatively charged Nafion and positively charged imidazole modified-graphene quantum dots (GQD-Im). We demonstrate here that Nafion/GQD-Im nanocoatings can combat the growth of representative Gram-positive and Gram-negative bacteria, and their excellent antibacterial performance is preserved after prolonged thermal treatment, indicating that the coatings can withstand dry heat sterilization without any decline in their properties. At the same time, the coatings show remarkable chemical and structural stability, while offering protection against UV-radiation as manifested by dye decomposition experiments. This novel type of nanocoatings demonstrates a unique combination of highly desirable characteristics, making them ideal candidates for applications related to active packaging for cosmetics and drugs, food processing, and disinfection of medical devices.

1 | Introduction

The introduction of antibiotics has revolutionized healthcare over the last century by dramatically mitigating the risk of pathogen infections across a diverse range of medical treatments [1]. However, their widespread and uncontrolled use has led to the emergence of antimicrobial resistance as a global threat for the public health with severe financial cost for the society [2, 3]. The vast majority of multidrug-resistant infections can be directly linked to nosocomial settings, with transmission predominantly occurring through contaminated high-touch surfaces and medical devices [4, 5]. Alongside research initiatives for the synthesis of a new generation of antibiotics [6] and efforts dedicated toward a more sensible antibiotic drug management, emphasis is placed on the development of antimicrobial coatings as an early intervention strategy in preventing transmission of the

pathogenic strains [7]. Heat-sterilizable antimicrobial coatings are particularly crucial in this context, as they retain antimicrobial efficacy following exposure to high temperatures ensuring long-term efficacy, safety, and reusability [8, 9].

In principle, antimicrobial coatings incorporate various compounds such as bacteriolytic enzymes, peptides, antibodies, drug molecules, and antiadhesive polymers along with photocatalytic and metallic nanoparticles [10–12]. Those biologically active agents to a greater or lesser extent are synthesized via laboratory-intensive procedures at a considerable cost, oftentimes raising concerns regarding their adverse environmental footprint and their high cytotoxicity [13]. In recent years, graphene (Gr)-based nanomaterials including pristine Gr graphene oxide (GO), reduced graphene oxide (rGO), and graphene quantum dots (GQDs) have garnered recognition as biocompatible antimicro-

This is an open access article under the terms of the [Creative Commons Attribution](https://creativecommons.org/licenses/by/4.0/) License, which permits use, distribution and reproduction in any medium, provided the original work is properly cited.

© 2025 The Author(s). *Nano Select* published by Wiley-VCH GmbH.

bial agents [14, 15] that can be produced at a large scale via green chemical procedures at a cost-effective manner [16–18]. The chemical modes of the inherent antimicrobial action of this class of materials rely on the induction of membrane stress, the production of reactive oxygen species (ROS), and arresting gene expression [19, 20]. Synergistic antibacterial activity between Gr-based and other types of nanomaterials or polymeric compounds has also been demonstrated in multicomponent systems [21], for example, GO/Ag [22] and GQD/ZnO [23] nanocomposites exhibit improved bactericidal effect compared to the individual components.

In this study, we present electrostatically assembled bilayers comprising positively charged imidazole modified-graphene quantum dots (GQD-Im) and negatively charged Nafion, a Teflon-based copolymer carrying ionic terminal groups. First, this system design capitalizes on the strong electrostatic interactions between Nafion and GQD-Im (Figure S1) to generate mechanically robust layer-by-layer (LbL) assemblies. Second, both Nafion and GQD-Im show high levels of thermal stability and are able to impart similar characteristics to their LbL assemblies. Third, Nafion is known for its capacity to create a bacterial exclusion zone on its surface [24] while GQDs demonstrate significant antimicrobial efficacy [15]. The nanocoatings presented here, not only, are able to suppress the population of representative Gram-positive and Gram-negative bacteria by more than 99%, and this performance is not compromised following extensive thermal treatment, but they also demonstrate superior UV barrier properties despite their transparent and colorless nature. In that sense, this study presents for the first time the development of structurally robust, waterborne coatings able to withstand dry heat sterilization, while offering remarkable shielding against pathogenic strains and UV radiation. To the best of our knowledge, no other type of polymer-based coating has been reported to simultaneously possess all those attractive characteristics.

2 | Materials and Methods

2.1 | Materials

A 10 wt% Nafion dispersion in water (hydrodynamic diameter 13.5 nm as shown in Figure S2) and a 20 wt% Nafion dispersion in a blend of low aliphatic alcohols (3-propanol, ethanol, and others) and water were acquired from Merck. The latter dispersion was used for spin-coating the crystal resonators, while the former was employed in all other experiments outlined in this study. For the dye decomposition experiments, hydrogen peroxide 30% (w/v) and neutral red dye were obtained from Thermo Fisher and Alfa Aesar, respectively. A 1 mg/mL dispersion of GQD-Im in water, with particles measuring 6 ± 3 nm as provided by the supplier, was obtained from ACS Material LLC. Both Nafion and GQDs-Im were used as received.

2.2 | Preparation of the Nafion/GQD-Imidazole Nanocomposite

Equal amounts of 0.01 wt% Nafion and 0.01 wt% GQD-Im (pH = 2) were mixed into a beaker, the mixture was subjected to ultrasonication for 15 min and was subsequently freeze dried.

2.3 | Quartz Crystal Microbalance With Dissipation Monitoring

The quartz crystal microbalance experiments with real-time dissipation monitoring (QCM-D) were carried out using a Q-sense E1 unit. Au-decorated crystal resonators with a diameter of 150 nm and fundamental resonance around 5 MHz were spin-coated with one drop of 0.5 wt% Nafion (in ethanol) before being loaded to a QCM-D flow cell, and the flow rate was adjusted to 0.2 mL/min. Aqueous dispersions of Nafion and GQD-Im were diluted in deionized water to achieve 0.25 wt% and 0.01 wt% solutions, respectively, and these solutions were used for the LbL assembly. The GQD-Im solution was subjected to ultrasonication before its introduction to the system.

The fundamental resonant frequency was determined by the crystal's initial equilibrium state in air, and the baseline of the hydrated surface was established by adding water at a constant flow rate.

On the basis of the Sauerbrey equation:

$$\Delta m = -(C/N)\Delta f \quad (1)$$

when a uniform layer with a mass of Δm is deposited, it causes a decrease in the crystal's resonant frequency by Δf . N represents the overtone number (all the data reported in this study correspond to $N = 3$), whereas C signifies the integrated sensitivity of the crystal, which is influenced by the inherent characteristics and thickness of the crystal [25]. The dissipation factor, denoted as D , is calculated by

$$D = E_d / (2\pi E_s) \quad (2)$$

where E_d represents the energy that is lost during a single oscillation cycle while E_s is the energy that the system has stored [26].

2.4 | Thermal Annealing

Coated QCM disks were placed within a Carbolite Gero ELF laboratory chamber at 200°C for 2 h.

2.5 | Zeta Potential (ζ Potential)

Zeta potential (ζ potential) measurements were carried out on a Malvern Panalytical Zetasizer Nano ZS with a 532 nm He–Ne laser at 25°C. Disposable folded capillary cells were used for the measurements. Before measurement, samples were subjected to ultrasonication for 5 min. Each measurement was repeated three times and their average value is reported.

2.6 | Dynamic Light Scattering (DLS)

DLS measurements were performed using a Malvern Panalytical Zetasizer Nano ZS with a 532 nm He–Ne laser at 25°C. The samples were filtered through 0.2 μ m Nylon membrane filters directly into the measuring cuvettes before measurement. The experiments were conducted in triplicate.

2.7 | Fourier Transform Infra-Red (FTIR) Spectroscopy

The Shimadzu IR Tracer-100 spectrophotometer, operating at room temperature, was used to record the FT-IR spectra of freeze dried samples. The spectrum for each sample was obtained by averaging 64 successive scans, spanning a range from 4000 to 500 cm^{-1} , with a resolution of 2 cm^{-1} .

2.8 | Raman Spectroscopy

Raman spectrum of GQD-Im was obtained using a Horiba Jobin Yvon HR800 Raman spectrometer within the range 800–2000 cm^{-1} . Samples were prepared by drop casting a 0.1 wt% GQD-Im solution on a glass slide, which was then left to dry overnight. A 532 nm air-cooled CLDS point mode diode laser was used, and the filter was adjusted to 10% to minimize the risk for structural damage.

2.9 | Ultraviolet-Visible (UV-Vis) Spectroscopy

UV-Vis spectra were acquired at room temperature using a Shimadzu UV-3600 spectrophotometer, employing Hellma Analytics quartz cuvettes with a 1.0 cm path length.

2.10 | Thermogravimetric Analysis (TGA)

TGA measures were performed using a TG 209 F1 Libra from Netzsch. The temperature was increased from room temperature to 1000°C at a heating rate of 15°C/min whilst under a constant nitrogen flow. The experiments were conducted in triplicate to ensure reproducibility.

2.11 | Contact Angle Measurements

Droplets of distilled water (5 μL) were deposited on the coated quartz crystals, and the contact angle was measured by means of an OptoSigma optical tensiometer at room temperature. The images were recorded 20 s following the deposition of the droplets, and the experiment was repeated five times for each sample.

2.12 | Scanning Electron Microscopy (SEM)

SEM imaging was performed using a Thermo Fisher Quattro SEM at an accelerating voltage of 3 kV. The sample analyzed was a coated QCM-D crystal, with the image presented in Figure S3.

2.13 | Transmission Electron Microscopy (TEM)

TEM imaging was carried out by means of JEOL JEM 1400 (Welwyn Garden City, UK) at an acceleration voltage of 80 kV, using samples that were dissolved in water and solution dispensed onto a carbon-filmed copper mesh grid and allowed to air dry overnight. The lattice spacings of the graphitic structure were measured using ImageJ software.

2.14 | Atomic Force Microscopy (AFM)

A Bruker Dimensions Icon atomic force microscope with a Nanoscope 6 controlled was used to acquire atomic force micrographs. The imaging was conducted in peak force tapping mode, employing silicone nitride cantilevers with a nominal spring constant of 0.4 N/m in air (SCANASYST-AIR, Bruker) and 0.7 N/m in fluid (SCANASYST-FLUID, Bruker). For each sample, images were recorded from a minimum of three separate locations with scan sizes of 10 μm . Average roughness (R_a) measurements were also collected at three distinct locations for each sample with scan sizes of 10 μm . Before measurement, a first-order flattening procedure was applied to process the images.

2.15 | UV-Induced Dye Degradation Experiments

The external walls of the borosilicate scintillation glass vials (20 mL, 25 mm in diameter) from Thermo Fisher were dip-coated using solutions of Nafion (0.1 wt%) and GQD-Im (0.01 wt%), generating five Nafion/GQD-Im bilayers on their surface. To evaluate the efficacy of those coatings in blocking UV radiation ($\lambda = 254 \text{ nm}$), 10 mL of a solution containing 65 μM neutral red dye and 6.7 mM H_2O_2 was introduced into the coated glass vial. Subsequently, the vials were exposed to UV radiation for 72 h, and the absorption at $\lambda = 525 \text{ nm}$ was monitored at predetermined time intervals. For comparison, uncoated vials were subjected to otherwise identical assessment. The experiments were conducted in triplicate and average values are reported in this study.

2.16 | Resistance to Friction Assessment

An Anton Paar modular compact rheometer 302e outfitted with a 50 mm parallel plate geometry was used to evaluate the behavior of the coated crystals under frictional forces. Polydimethylsiloxane (PDMS) was used to mimic human skin as suggested in previous studies [27, 28]. PDMS disks with 40 mm diameter and 4 mm thickness sourced from Silex Ltd were securely affixed to the upper plate geometry, and the coated QCM crystals were attached to the bottom plate using double-sided adhesive tape. Rotational shear experiments were carried out at zero gap, applying a constant shear rate for 60 s after which each crystal was submerged in 3 mL of water for 10 min. The UV-Vis spectrum of this water was then analyzed to detect potential traces of detached GQD-Im. The test was repeated at incrementally higher shear rates ($\dot{\gamma}$) (i.e., $\dot{\gamma} = 1 \times 10^5, 2 \times 10^5, 3 \times 10^5, \text{ and } 4 \times 10^5 \text{ s}^{-1}$) until GQD-Im was spectrometrically detected in the aqueous suspension or until the upper limits of shear rate were achieved. The experiments were conducted in triplicate to ensure reproducibility.

2.17 | Antimicrobial Testing

2.17.1 | Preparation of Bacterial Cultures

In 250 mL Erlenmeyer flasks with 25 mL nutrient broth, bacterial cultures were cultivated and incubated for 24 h at 37°C in a SciQuip Incu-Shake MIDI orbital shaker (SciQuip Ltd, Newtown, Wem, Shropshire, UK) set to 200 rpm. The cultures

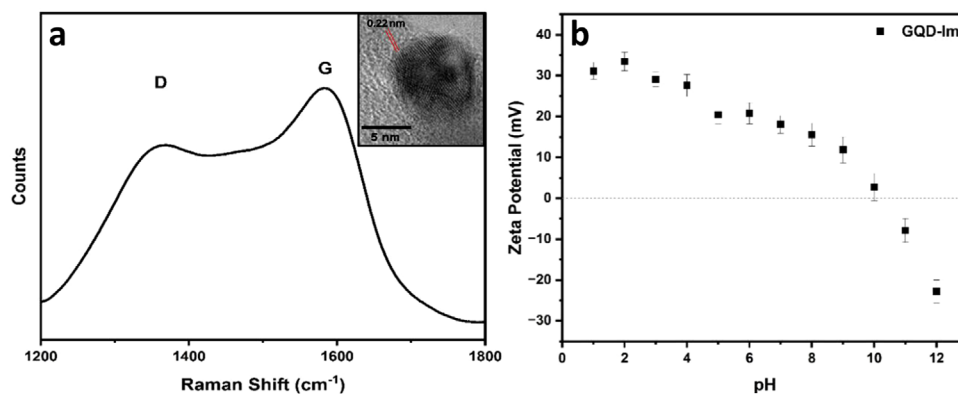


FIGURE 1 | (a) Raman spectrum and TEM image (insert) of GQD-Im, (b) zeta potential of 0.005 wt% GQD-Im in water at various pH values. GQD-Im, imidazole modified-graphene quantum dot; TEM, transmission electron microscopy.

were centrifuged for 10 min at 4000 rpm, the supernatant was removed, and 20 mL of 1/4 strength Ringer's solution was added. The tubes were vortexed followed by centrifugation for 10 min at 4000 rpm, and the supernatant disposed of 2 mL of 1/4 strength Ringer's solution was introduced into the tubes, which were then subjected to a final round of vortexing. Cultures, once resuspended, were diluted in nutrient broth to achieve an absorbance reading that matched a 0.5 McFarlane standard using a Biochrom WPA S800 visible spectrophotometer (Biochrom Ltd, Cambridge, UK). This diluted culture was then used as the inoculum for the disk tests.

2.17.2 | Bacterial Inoculation in the Absence and Presence of Nanocoatings

The testing method was attained from the literature and was used to assess the antimicrobial efficacy of the coatings [29]. Each sample disk (uncoated, Nafion coated, Naf/GQD-Im coated, and annealed Naf/GQD-Im coated) was allocated to one of the twelve wells using a random number generator. Each of these wells was lined with sterile aluminum foil to facilitate the removal of disks and prevent bacterial run-off. An extra well was filled with 1 mL of sterile, distilled, deionized water to mitigate the dehydration of the samples. Each disk was inoculated with 200 μ L of bacterial culture as prepared in Section 2.17.1 and then incubated for 20 h at a temperature of 37°C. After the incubation period, each disk, along with the foil, was moved into 9.8 mL of 1/4 Ringer's solution and then sonicated for a duration of 10 min. The resulting solution underwent successive dilutions with 100 μ L of the sample solution being diluted into 900 μ L of quarter-strength Ringer's solution. A 100 μ L aliquot of each sample was spread onto individual nutrient agar plates, with each dilution being plated in triplicate. The plates were then incubated for 20 h at 37°C, after which the colonies were counted. For each type of coating, five crystals were assessed and the average values were determined.

3 | Results and Discussion

The Raman spectrum of GQD-Im (Figure 1a) displays the D band at 1369 cm^{-1} and the G band at 1587 cm^{-1} , stemming

from the stretching vibrations of carbon atoms in the sp^3 and sp^2 hybridization states, respectively. Their intensity ratio I_D/I_G equals 0.78, implying that the GQD-Im possesses a well-ordered graphitic framework with minimal structural defects [30]. This high degree of graphitization is further corroborated by the TEM image (insert in Figure 1a), which shows a GQD-Im particle approximately 8 nm in size and exhibits lattice spacings close to 0.22 nm corresponding to the graphitic structure, consistent with values reported in the literature [31, 32].

At the same time, the aqueous dispersions of GQD-Im exhibit excitation-wavelength (λ_{ex}) dependent fluorescent emission, that is, characteristic for this class of materials (Figure S4a) [33, 34]. The strongest emission signal is observed at $\lambda_{\text{ex}} = 380$ nm, but the emissive peaks shift at higher wavelengths and their intensity gradually diminishes upon further λ_{ex} increase. The UV-Vis spectrum of aqueous dispersion of GQD-Im (Figure S4b) is dominated by a sharp peak at 200 nm corresponding to π - π^* transitions of aromatic C-C [35, 36], while Nafion exhibits minimal absorbance in this region, as discussed previously [37, 38].

The zeta potential (ζ) of aqueous dispersions of GQD-Im shown in Figure 1b shows positive values between pH = 1 ($\zeta = 31.1$ mV) and pH = 10 ($\zeta = 2.7$ mV), while negative values are observed at pH = 11 ($\zeta = -7.9$ mV) and pH = 12 ($\zeta = -22.8$ mV). Those trends can be explained in terms of gradual deprotonation of the surface groups (hydroxyl, carboxyl, amine group of the imidazole ring) at higher pH values, as reported in similar systems [39, 40]. For all subsequent experiments reported herein the pH of GQD-Im was set to 2 ($\zeta = 33.5$ mV) in order to maximize electrostatic interactions with Nafion that shows pH = 2.7 ($\zeta = -54.8$ mV).

The FTIR spectrum of GQD-Im (black line in Figure 2) displays peaks at 1680, 1380, 1160, 1030, 787, and 613 cm^{-1} representing C=O stretching, C-N stretching (imidazole ring amine), C-N stretching, C-O stretching, C-H bending, and C-H stretching [41-43], respectively. The Nafion FTIR spectrum (blue line in Figure 2) shows peaks placed at 1202, 1143, 1056, 975, 629, and 512 cm^{-1} corresponding to asymmetric stretching of C-F, symmetric stretching of C-F, stretching of S=O, stretching of C-O-C, stretching of C-S, and bending of O-S-O, respectively

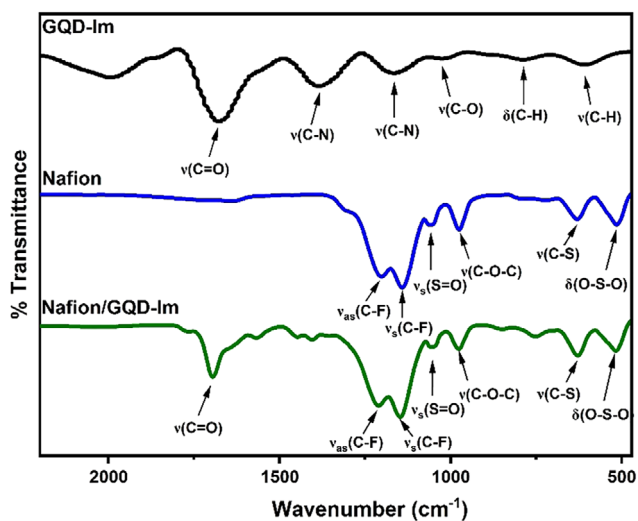


FIGURE 2 | FTIR spectra of GQD-Im (black line), Nafion (blue line), and Nafion/GQD-Im nanocomposite (green line). FTIR, Fourier transform infra-red; GQD-Im, imidazole modified-graphene quantum dot.

[44, 45]. Interestingly, the Nafion/GQD-Im FTIR spectrum (green line in Figure 2) shows that the peaks assigned to C–F asymmetric stretching, C–F symmetric stretching, and S–O stretching are centered to 1210, 1147, and 1058 cm^{-1} indicating 8 and 4 cm^{-1} displacement compared to pristine Nafion, respectively. This observation points to the reorganization of the Nafion backbone arising from strong electrostatic interactions between the sulfonic acid and imidazole groups [46]. It has been demonstrated that pyrrole-like nitrogen atoms from imidazole group can donate protons to the oxygen of negatively charged sulfonate groups of Nafion, whilst pyridine-like nitrogen atoms accept protons from sulfonic acid groups, thereby promoting the formation of hydrogen bonds [47]. The displacement of S=O bond in particular has been also reported in imidazole functionalized silica/Nafion composite membranes wherein interactions between Nafion's sulfonic acid groups and imidazole moieties resulted in the formation of ionic clusters [48].

The TGA thermogram of Nafion shown in Figure 3 reflects the action of three major thermal events associated with the water evaporation at temperatures below 100°C, the sulfonic group decomposition starting at 300°C and the degradation of the tetrafluoroethylene backbone at temperatures above 380°C [49]. Moreover, the TGA profile of GQD-Im suggests a rather limited removal of absorbed water at temperatures below 100°C, the decomposition of imidazole and oxygen containing groups within the temperature range 100–250°C, while the carbon backbone breakdown commences at 260°C [50]. The Nafion/GQD-Im demonstrates a thermal profile in analogy to that observed for pristine Nafion and retains more than 90% of its weight at 300°C and the decomposition of sulfonic groups commences at 20°C higher compared to pristine and this enhanced thermal stability can be attributed to the sulfonic acid/imidazole interactions. More broadly, by virtue of its amphiphilic nature Nafion shows strong interactions with carbon nanotubes [51], GO [52], GQDs [53], and carbon dots (C-dots) [54].

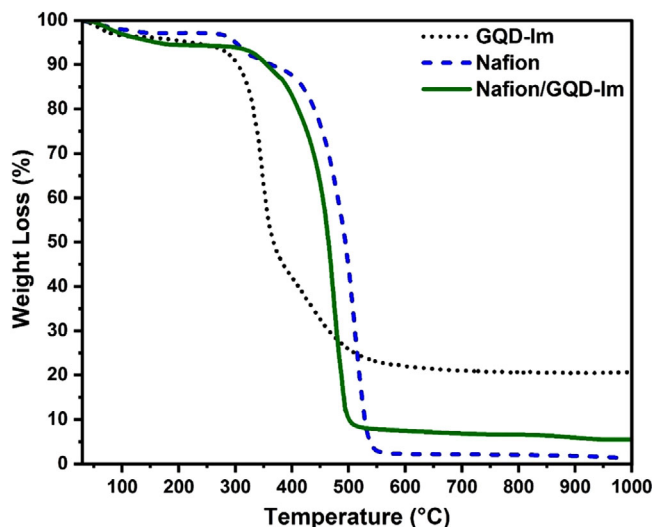


FIGURE 3 | TGA thermograms of GQD-Im, Nafion, and Nafion/GQD-Im nanocomposite under nitrogen flow. GQD-Im, imidazole modified-graphene quantum dot; TGA, thermogravimetric analysis.

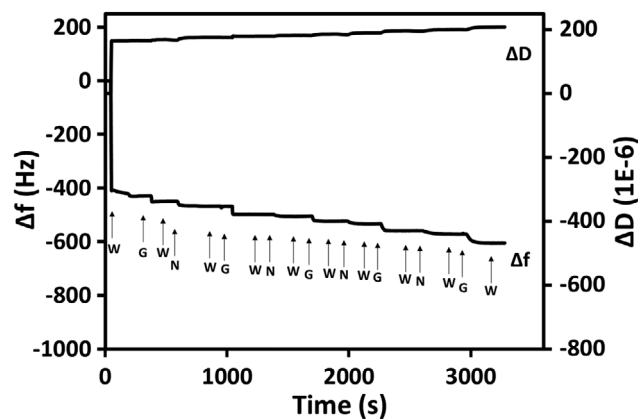


FIGURE 4 | Time course of the build-up (Naf/GQD-Im)₅ during QCM-D experiments. The letters “W”, “G”, and “N” signify the injection of water, GQD-Im, and Nafion, respectively. QCM-D, quartz crystal microbalance experiments with real-time dissipation monitoring; GQD-Im, imidazole modified-graphene quantum dot.

QCM-D experiments were designed in order to monitor in real time the build-up of nanocoatings via LbL assembly, a versatile technique with precise nanoscale control that relies on the sequential deposition of oppositely charged structural units [55]. The QCM-D sensorgram shown in Figure 4 illustrates the assembly of five Nafion/GQD-Im bilayers, denoted hereafter as (Naf/GQD-Im)₅ on a Nafion pretreated crystal resonator. The injection of water to the precoated crystal results in a pronounced decrease in oscillating frequency (Δf) along with a corresponding rise in the dissipation factor (D), consistent with significant swelling of the ionic channels of Nafion [56]. The subsequent injection of GDD-Im on the hydrated Nafion membrane results in a further decrease in Δf and the QCM-D sensorgram reveals a steady build-up of five successive Nafion/GQD-Im bilayers as a direct consequence of the strong electrostatic interactions between Nafion and GQD-Im. For reference, it is noted that the

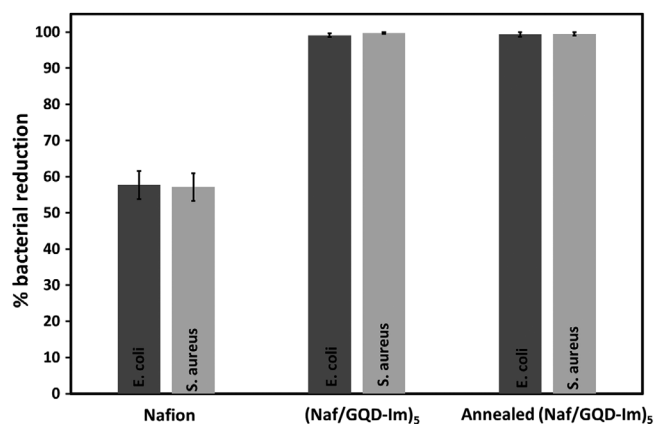


FIGURE 5 | Reduction percentages of *E. coli* and *S. aureus* cultures exposed to Nafion, (Naf/GQD-Im)₅, and annealed-(Naf/GQD-Im)₅ QCM-D nanocoatings. QCM-D, quartz crystal microbalance experiments with real-time dissipation monitoring; GQD-Im, imidazole modified-graphene quantum dot.

introduction of protonated imidazole rings to Nafion membranes results in further enlargement of the ionic channels [47].

The thus prepared (Naf/GQD-Im)₅ coatings were immersed in water, ethanol, and acetone for 10 min under ultrasonication and subsequent UV-Vis and fluorescence spectroscopy analysis of the solvents showed no detectable traces of GQD-Im, indicating the stability of the coatings in these environments. Moreover, the crystals were thermally treated at 200°C for 2 h, thus giving rise to annealed-(Naf/GQD-Im)₅ that were also found to be stable against water, ethanol, and acetone when tested under similar conditions. During soft tribological studies, (Naf/GQD-Im)₅ and annealed-(Naf/GQD-Im)₅ coatings were subjected to shear rates up to $\dot{\gamma} = 4 \times 10^5 \text{ s}^{-1}$ and were subsequently immersed in water. On the basis of the UV and fluorescence spectra of the eluent water, no traces of GQD-Im were detected, indicating that the coatings resist detachment even under substantial friction forces.

As shown in Figure 5, the (Naf/GQD-Im)₅ coatings inhibit *E. coli* and *Staphylococcus aureus* growth by 99.1% and 99.7%, respectively, while under otherwise identical conditions Nafion coatings were found to inhibit the growth of *E. coli* and *S. aureus* by 57.7% and 57.1%, respectively. The excellent antimicrobial performance displayed by (Naf/GQD-Im)₅ coatings points to the synergistic action exerted by Nafion, imidazole groups, and GQD.

First, Nafion-coated stainless steel shows reduced adhesion of *E. coli* and *Bacillus subtilis* by 70%–75% compared to the uncoated surface [29, 57]. Teflon-reinforced Nafion membrane showed significant activity against *S. aureus* and *E. coli* and this behavior was further improved in the presence of Ag–Cu coating [58]. The nonequilibrium phenomena that take place in the bacterial exclusion zone of Nafion have been monitored by means of confocal laser scanning microscope suggesting only sporadic cell attachment during the first 24 h of incubation, followed by significant contamination after a further 24 h incubation [24]. A recent report indicated that Nafion-based membranes even with a positive surface zeta potential can reduce the growth of Gram-negative and Gram-positive bacteria by more than 99%, an

observation that cannot be explained solely in terms of exclusion zone effects [59].

Second, imidazolium derivatives are the active compounds in several antimicrobial formulations that show remarkable efficiency against Gram-positive bacteria. Their cationic nature induces electrostatic interactions with the negatively charged bacterial cell wall leading to membrane disruption and subsequent cell death [60, 61]. Moreover, imidazole-based antibiotics were shown to arrest the function of the nitric oxide dioxygenase of microbial flavohemoglobin [62]. Polyimidazolium salt-based coatings demonstrated enhanced antibacterial activity against methicillin-resistant *S. aureus* (MRSA) while imidazole functionalized hyperbranched polyester coatings were effective against MRSA and *B. subtilis* [63, 64]. Incorporation of imidazole modified carboxylated GO into polyurethane coatings resulted in nanocomposites with excellent antimicrobial activity in addition to antifouling, anticorrosion, and self-healing functions [65].

Third, unmodified GQDs have demonstrated the ability to prevent bacterial growth; however, the minimum inhibitory concentrations required were as high as 256 µg/mL for *E. coli* and 512 µg/mL for *S. aureus* [66]. Functionalized GQDs have proven to be more effective antimicrobial agents and their overall mechanism can be ascribed to cell membrane stress upon contact, electron transport disruption between bacterial cells and production of ROS [19, 67]. N-doped GQDs in particular have demonstrated enhanced antimicrobial efficacy, and this is attributed to their superior ROS generation compared to N-free counterparts [68]. In a previous study, the GQD-Im displayed over 90% disinfection rates against three Gram-positive bacteria (*S. aureus*, methicillin-resistant *S. aureus*, and *S. epidermidis*) within 3 h. However, the antimicrobial activity against the Gram-negative bacterium *E. coli* was reported to be only 24.2% within the same timeframe [39]. A nanocomposite comprising histidine functionalized GQDs (thus containing imidazole side chains) and titanium dioxide (TiO₂) nanorods was prepared for dental applications, and it was found that the nanocomposite was able to reduce *Streptococcus mutans*, a Gram-positive bacterium by 97.8% [69].

Significantly, the antibacterial performance of (Naf/GQD-Im) was not compromised upon prolonged thermal treatment (2 h at 200°C), given that annealed-(Naf/GQD-Im)₅ coatings inhibit the growth of *E. coli* by 99.3% and *S. aureus* by 99.1%. Such remarkable thermal resistance has been previously reported by our group for LbL assemblies comprising alternate layers of Nafion and amine functionalized GO (Naf/GO-NH₂)₅ [70]. As shown in Figure 6, the water contact angle of Nafion decreases from 100.7° to 106.5° upon thermal annealing, an effect that has been attributed to the partial withdrawal of the sulfonic pendant groups from surface areas, thus enhancing the hydrophobic character of the membrane [71]. Likewise, the water contact angle of (Naf/GQD-Im)₅ increases from 70.5° to 108.2° upon thermal annealing (Figure 6) due to surface rearrangements primarily related to Nafion. Similar effects have been observed in relation to thermal annealing of (Naf/GO-NH₂)₅ [70].

As shown in Figure 7a, the surface morphology of (Naf/GQD-Im)₅ as monitored via AFM imaging is dominated by the presence of aggregates that give rise to surface roughness $R_a = 3.7 \pm 0.5 \text{ nm}$,

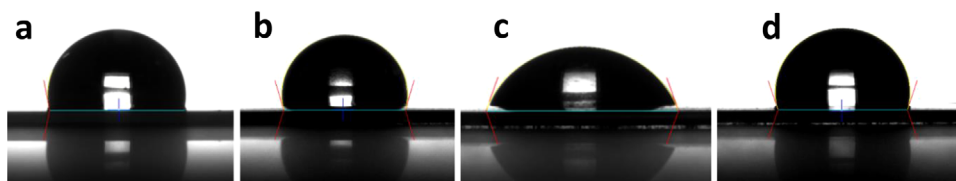


FIGURE 6 | Contact angle of water droplets deposited on: (a) Nafion, (b) annealed-Nafion, (c) (Naf/GQD-Im)₅, and (d) annealed-(Naf/GQD-Im)₅. GQD-Im, imidazole modified-graphene quantum dot.

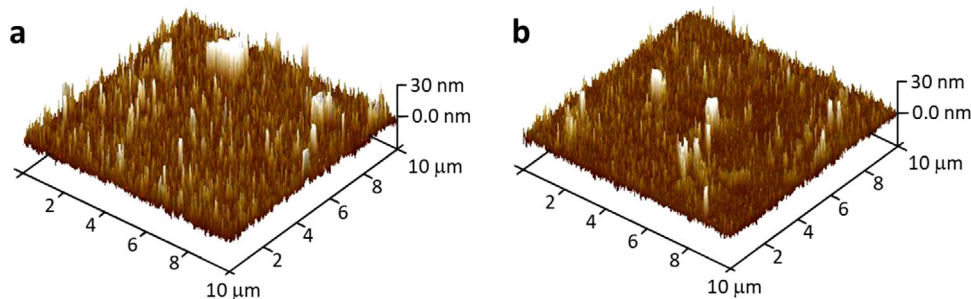


FIGURE 7 | 3D AFM images of: (a) (Naf/GQD-Im)₅ and (b) annealed-(Naf/GQD-Im)₅ coatings. AFM, atomic force microscopy; GQD-Im, imidazole modified-graphene quantum dot.

and this value is reduced to $R_a = 3.3 \pm 0.2$ nm for the annealed-(Naf/GQD-Im)₅ (Figure 7b), though this change might not reach statistical significance. For reference, it is noted that average roughness between 28 and 37 nm was reported in LbL chitosan/C-dots assemblies [72].

The development of UV-resistant coatings is crucial for a series of challenging applications including packaging for food, cosmetics and drugs, optical devices, contact lenses, eyeglasses, window protection films, smart textiles, aerospace, etc. Ideally, the coatings should be able to block UV rays in order to provide protection against photooxidation and photodegradation effects, while fully retaining their colorless nature and their transparency within the visible area of the spectrum to allow direct observation of the surface under them. To that end, Gr-based nanomaterials are explored as UV-blocking agents in food packaging with the potential to enhance the organoleptic qualities and the shelf-life of food products, without compromising transparency. For example, GO/cellulose acetate composite membranes show 57% UV-blocking capacity and 79% visible light transparency [73], while GO/polyacrylonitrile composite showed the UV-A and UV-B blocking capacity close to 57% and 71%, respectively, with a visible light transmittance close to 77% [74].

It is interesting to note that the (Naf/GQD-Im)₅ coatings presented in this study appear colorless and transparent from visible radiation as evidenced in Figure S5. The degradation profiles of neutral red dye (in the presence of hydrogen peroxide) enclosed in noncoated and (Naf/GQD-Im)₅ coated glass vials under UV exposure are compared in Figure 8. The results suggest that the coating offers shielding against UV radiation, giving rise to 38% of dye decomposition after 72 h of UV exposure, compared to 57% for the uncoated vial. Previous studies demonstrated that GQDs/polyvinyl alcohol (PVA) [75], GQDs/PVA/chitosan films [76], and GQD/PVA films on polyethylene terephthalate (PET) bottles [77] all show excellent UV-blocking capacity

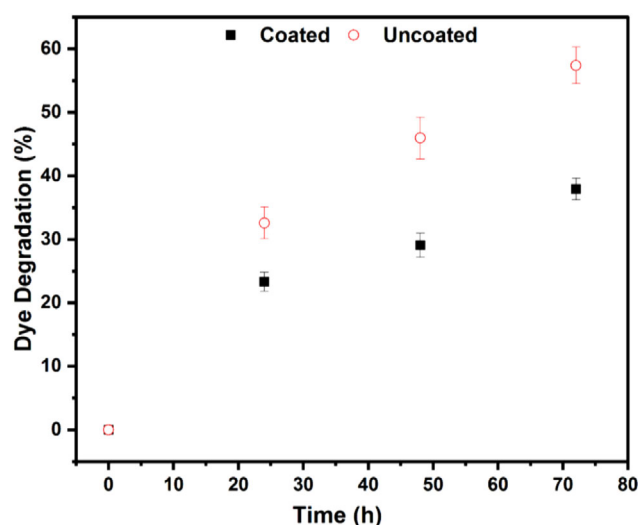


FIGURE 8 | Degradation percentage of neutral red dye (in the presence of hydrogen peroxide) within (Naf/GQD-Im)₅ coated and noncoated glass vials after UV exposure (254 nm) at intervals of 0, 24, 48, and 72 h. GQD-Im, imidazole modified-graphene quantum dot.

(higher than 80%), without compromising their transparency from visible light. At the same time, the introduction of GQDs to starch/gelatine films decreases transmittance in both the visible range (660 nm) and UV region (280 nm) and endowed greater antibacterial activity against Gram-positive compared to Gram-negative strains [78].

4 | Conclusion

In conclusion, we present for the first time the development of GQDs-based coatings that can reduce the population of *E. coli* and *S. aureus* by more than 99%, and this excellent antimicrobial

behavior is preserved following thermal treatment at 200°C for 2 h. At the same time, the nanocoatings offer significant protection against UV radiation, while showing remarkable stability in the presence of solvents. The combination of those promising performance characteristics coupled with their waterborne, nontoxic, colorless, and transparent nature makes this new type of coatings suitable for a range of applications such as surgical and medical equipment, smart packaging for products prone to degradation, and food processing surfaces. Further studies in real-world environments will provide insights regarding the performance of the coatings under adverse environmental conditions (high humidity, high salinity) and will elucidate their behavior with respect to biofilm formation.

Supporting Information

Supporting Information is available from the Wiley Online Library or from the author.

Acknowledgments

Spyridon Gavalas was supported by the University Alliance Doctoral Training Alliance under the Marie Skłodowska-Curie COFUND scheme. Financial support from the Higher Education Innovation Fund (Research England) and UCLan Research Centre for Smart Materials is gratefully acknowledged.

Conflicts of Interest

The authors declare no conflicts of interest.

Data Availability Statement

The data that support the findings of this study are available from the corresponding author upon reasonable request.

References

1. T. J. Hall, V. M. Villapún, O. Addison, et al., “A Call for Action to the Biomaterial Community to Tackle Antimicrobial Resistance,” *Biomaterials Science* 8, no. 18 (2020): 4951–4974, <https://doi.org/10.1039/d0bm01160f>.
2. M. A. Abushaheen, F. A. J. Muzaheed, M. Alosaimi, et al., “Antimicrobial Resistance, Mechanisms and Its Clinical Significance,” *Disease-a-Month* 66, no. 6 (June 2020): 100971, <https://doi.org/10.1016/j.disamonth.2020.100971>.
3. G. Ferreres, K. Ivanova, I. Ivanov, and T. Tzanov, “Nanomaterials and Coatings for Managing Antibiotic-Resistant Biofilms,” *Antibiotics* 12, no. 2 (February 2023): 310, <https://doi.org/10.3390/antibiotics12020310>.
4. J. Butler, R. D. Handy, M. Upton, and A. Besinis, “Review of Antimicrobial Nanocoatings in Medicine and Dentistry: Mechanisms of Action, Biocompatibility Performance, Safety, and Benefits Compared to Antibiotics,” *ACS Nano* 17, no. 8 (April 2023): 7064–7092, <https://doi.org/10.1021/acsnano.2c12488>.
5. M. Salwiczek, Y. Qu, J. Gardiner, et al., “Emerging Rules for Effective Antimicrobial Coatings,” *Trends in Biotechnology* 32, no. 2 (February 2014): 82–90, <https://doi.org/10.1016/j.tibtech.2013.09.008>.
6. P. J. Weldick, A. Wang, A. F. Halbus, and V. N. Paunov, “Emerging Nanotechnologies for Targeting Antimicrobial Resistance,” *Nanoscale* 14, no. 11 (2022): 4018–4041, <https://doi.org/10.1039/d1nr08157h>.
7. F. Pietsch, A. J. O'Neill, A. Ivask, et al., “Selection of Resistance by Antimicrobial Coatings in the Healthcare Setting,” *Journal of Hospital Infection* 106, no. 1 (September 2020): 115–125, <https://doi.org/10.1016/j.jhin.2020.06.006>.
8. N. P. Tipnis and D. J. Burgess, “Sterilization of Implantable Polymer-Based Medical Devices: A Review,” *International Journal of Pharmaceutics* 544, no. 2 (June 2018): 455–460, <https://doi.org/10.1016/j.ijpharm.2017.12.003>.
9. N. G. Skrzypczak, N. G. Tanikella, and J. M. Pearce, “Open Source High-Temperature Reprap for 3-D Printing Heat-Sterilizable PPE and Other Applications,” *HardwareX* 8 (October 2020): e00130, <https://doi.org/10.1016/j.ohx.2020.e00130>.
10. S. Aslan, J. Määttä, B. Z. Haznedaroglu, et al., “Carbon Nanotube Bundling: Influence on Layer-by-Layer Assembly and Antimicrobial Activity,” *Soft Matter* 9, no. 7 (2013): 2136, <https://doi.org/10.1039/c2sm27444b>.
11. P. Singha, J. Locklin, and H. Handa, “A Review of the Recent Advances in Antimicrobial Coatings for Urinary Catheters,” *Acta Biomaterialia* 50 (March 2017): 20–40, <https://doi.org/10.1016/j.actbio.2016.11.070>.
12. A. Shahid, B. Aslam, and S. Muzammil, “The Prospects of Antimicrobial Coated Medical Implants,” *Journal of Applied Biomaterials & Functional Materials* 19 (January 2021): 22808000211040304, <https://doi.org/10.1177/22808000211040304>.
13. H. Sun, N. Gao, K. Dong, J. Ren, and X. Qu, “Graphene Quantum Dots-Band-AIDS Used for Wound Disinfection,” *ACS Nano* 8, no. 6 (June 2014): 6202–6210, <https://doi.org/10.1021/nm501640q>.
14. M. Azizi-Lalabadi, H. Hashemi, J. Feng, and S. M. Jafari, “Carbon Nanomaterials Against Pathogens; the Antimicrobial Activity of Carbon Nanotubes, Graphene/Graphene Oxide, Fullerenes, and Their Nanocomposites,” *Advances in Colloid and Interface Science* 284 (October 2020): 102250, <https://doi.org/10.1016/j.cis.2020.102250>.
15. B. Z. Ristic, M. M. Milenkovic, I. R. Dakic, et al., “Photodynamic Antibacterial Effect of Graphene Quantum Dots,” *Biomaterials* 35, no. 15 (May 2014): 4428–4435, <https://doi.org/10.1016/j.biomaterials.2014.02.014>.
16. J. Shen, Y. Zhu, X. Yang, and C. Li, “Graphene Quantum Dots: Emergent Nanolights for Bioimaging, Sensors, Catalysis and Photovoltaic Devices,” *Chemical Communications* 48, no. 31 (2012): 3686, <https://doi.org/10.1039/c2cc00110a>.
17. S. N. Baker and G. A. Baker, “Luminescent Carbon Nanodots: Emergent Nanolights,” *Angewandte Chemie International Edition* 49, no. 38 (August 2010): 6726–6744, <https://doi.org/10.1002/anie.200906623>.
18. Z. Fan, Y. Li, X. Li, et al., “Surrounding Media Sensitive Photoluminescence of Boron-Doped Graphene Quantum Dots for Highly Fluorescent Dyed Crystals, Chemical Sensing and Bioimaging,” *Carbon* 70 (April 2014): 149–156, <https://doi.org/10.1016/j.carbon.2013.12.085>.
19. K. Rajendiran, Z. Zhao, D.-S. Pei, and A. Fu, “Antimicrobial Activity and Mechanism of Functionalized Quantum Dots,” *Polymers* 11, no. 10 (October 2019): 1670, <https://doi.org/10.3390/polym11101670>.
20. A. Anand, B. Unnikrishnan, S.-C. Wei, C. P. Chou, L.-Z. Zhang, and C.-C. Huang, “Graphene Oxide and Carbon Dots as Broad-Spectrum Antimicrobial Agents—A Minireview,” *Nanoscale Horizons* 4, no. 1 (2019): 117–137, <https://doi.org/10.1039/c8nh00174j>.
21. P. Kumar, P. Huo, R. Zhang, and B. Liu, “Antibacterial Properties of Graphene-Based Nanomaterials,” *Nanomaterials* 9, no. 5 (May 2019): 737, <https://doi.org/10.3390/nano9050737>.
22. T. Vi, S. Kumar, J.-H. Pang, Y.-K. Liu, D. Chen, and S. Lue, “Synergistic Antibacterial Activity of Silver-Loaded Graphene Oxide Towards *Staphylococcus aureus* and *Escherichia coli*,” *Nanomaterials* 10, no. 2 (February 2020): 366, <https://doi.org/10.3390/nano10020366>.
23. J. Liu, M. D. Rojas-Andrade, G. Chata, et al., “Photo-Enhanced Antibacterial Activity of ZnO/Graphene Quantum Dot Nanocomposites,” *Nanoscale* 10, no. 1 (2018): 158–166, <https://doi.org/10.1039/c7nr07367d>.
24. Y. Cheng and C. I. Moraru, “Long-Range Interactions Keep Bacterial Cells From Liquid-Solid Interfaces: Evidence of a Bacteria Exclusion Zone Near Nafion Surfaces and Possible Implications for Bacterial

- Attachment," *Colloids and Surfaces B: Biointerfaces* 162 (February 2018): 16–24, <https://doi.org/10.1016/j.colsurfb.2017.11.016>.
25. G. Z. Sauerbrey, "The Use of Quartz Oscillators for Weighing Thin Layers and for Microweighing," *Zeitschrift für Physik* 155 (1959): 206–222, <https://doi.org/10.1007/BF01337937>.
26. M. Rodahl, F. Höök, A. Krozer, P. Brzezinski, and B. Kasemo, "Quartz Crystal Microbalance Setup for Frequency and Q-Factor Measurements in Gaseous and Liquid Environments," *Review of Scientific Instruments* 66, no. 7 (July 1995): 3924–3930, <https://doi.org/10.1063/1.1145396>.
27. K. Timm, C. Myant, H. A. Spikes, and M. Grunze, "Particulate Lubricants in Cosmetic Applications," *Tribology International* 44, no. 12 (November 2011): 1695–1703, <https://doi.org/10.1016/j.triboint.2011.06.017>.
28. J. Lee, J. Lu, A. Potanin, and C. Boyke, "Prediction of Tactile Sensory Attributes of Facial Moisturizers by Rheology and Tribology," *Biotribology* 28 (December 2021): 100201, <https://doi.org/10.1016/j.biotri.2021.100201>.
29. L. J. Zhong, L. Q. Pang, L. M. Che, X. E. Wu, and X. D. Chen, "Nafion Coated Stainless Steel for Anti-Biofilm Application," *Colloids and Surfaces B: Biointerfaces* 111 (November 2013): 252–256, <https://doi.org/10.1016/j.colsurfb.2013.05.039>.
30. E. Dervishi, Z. Ji, H. Htoon, M. Sykora, and S. K. Doorn, "Raman Spectroscopy of Bottom-Up Synthesized Graphene Quantum Dots: Size and Structure Dependence," *Nanoscale* 11, no. 35 (2019): 16571–16581, <https://doi.org/10.1039/c9nr05345j>.
31. S. Sarkar, D. Gandla, Y. Venkatesh, et al., "Graphene Quantum Dots From Graphite by Liquid Exfoliation Showing Excitation-Independent Emission, Fluorescence Upconversion and Delayed Fluorescence," *Physical Chemistry Chemical Physics* 18, no. 31 (2016): 21278–21287, <https://doi.org/10.1039/c6cp01528j>.
32. V.-A. Thai, T.-B. Nguyen, C. P. Huang, et al., "Graphene Quantum Dots (GQDs) Decorated Zeolitic Imidazole Framework-67 (zif67) Electrode for the In-Situ Oxidation of Ciprofloxacin in Water," *Environmental Technology & Innovation* 30 (May 2023): 103039, <https://doi.org/10.1016/j.eti.2023.103039>.
33. A. Kelarakis, "Graphene Quantum Dots: In the Crossroad of Graphene, Quantum Dots and Carbogenic Nanoparticles," *Current Opinion in Colloid & Interface Science* 20, no. 5–6 (October 2015): 354–361, <https://doi.org/10.1016/j.cocis.2015.11.001>.
34. J. D. Stachowska, A. Murphy, C. Mellor, et al., "A Rich Gallery of Carbon Dots Based Photoluminescent Suspensions and Powders Derived by Citric Acid/Urea," *Scientific Reports* 11, no. 1 (May 2021): 10554, <https://doi.org/10.1038/s41598-021-89984-w>.
35. J. Sun, S. Yang, and Z. Wang, "Ultra-High Quantum Yield of Graphene Quantum Dots: Aromatic-Nitrogen Doping and Photoluminescence Mechanism," *Particle & Particle Systems Characterization* 32, no. 4 (November 2014): 434–440, <https://doi.org/10.1002/ppsc.201400189>.
36. Q. Cai, W. Sheng, J. Yang, et al., "Synergistic Passivation and Down-Conversion by Imidazole-Modified Graphene Quantum Dots for High Performance and UV-resistant Perovskite Solar Cells," *Advanced Functional Materials* 33, no. 43 (June 2023), <https://doi.org/10.1002/adfm.202304503>.
37. C.-H. Lin, C.-H. Wan, and W. Wu, "Suppressing Methanol Crossover With Nanometer-Sized PT3SN Particles Self-Assembled on a Nafion Membrane Surface," *International Journal of Electrochemical Science* 8, no. 6 (June 2013): 8236–8251, [https://doi.org/10.1016/s1452-3981\(23\)12883-5](https://doi.org/10.1016/s1452-3981(23)12883-5).
38. E. I. Santiago, R. A. Isidoro, M. A. Dresch, B. R. Matos, M. Linardi, and F. C. Fonseca, "Nafion–TiO₂ Hybrid Electrolytes for Stable Operation of PEM Fuel Cells at High Temperature," *Electrochimica Acta* 54, no. 16 (June 2009): 4111–4117, <https://doi.org/10.1016/j.electacta.2009.02.040>.
39. Y. Fang, L. Zhuo, H. Yuan, H. Zhao, and L. Zhang, "Construction of Graphene Quantum Dot-Based Dissolving Microneedle Patches for the Treatment of Bacterial Keratitis," *International Journal of Pharmaceutics* 639 (May 2023): 122945, <https://doi.org/10.1016/j.ijpharm.2023.122945>.
40. D. Kurniawan and W.-H. Chiang, "Microplasma-Enabled Colloidal Nitrogen-Doped Graphene Quantum Dots for Broad-Range Fluorescent pH Sensors," *Carbon* 167 (October 2020): 675–684, <https://doi.org/10.1016/j.carbon.2020.05.085>.
41. L. Ruiyi, J. Yanhong, W. Qinsheng, et al., "Serine and Histidine-Functionalized Graphene Quantum Dot With Unique Double Fluorescence Emission as a Fluorescent Probe for Highly Sensitive Detection of Carbendazim," *Sensors and Actuators B: Chemical* 343 (September 2021): 130099, <https://doi.org/10.1016/j.snb.2021.130099>.
42. X. Wang, D. Wang, Y. Guo, et al., "Imidazole Derivative-Functionalized Carbon Dots: Using as a Fluorescent Probe for Detecting Water and Imaging of Live Cells," *Dalton Transactions* 44, no. 12 (2015): 5547–5554, <https://doi.org/10.1039/c5dt00128e>.
43. B. Mehrdad-Vahdati, S. Pourhashem, M. Sedghi, et al., "A Novel Aspect of Functionalized Graphene Quantum Dots in Cytotoxicity Studies," *Toxicology In Vitro* 61 (December 2019): 104649, <https://doi.org/10.1016/j.tiv.2019.104649>.
44. T. Hwang, V. Palmre, J. Nam, D.-C. Lee, and K. J. Kim, "A New Ionic Polymer–Metal Composite Based on Nafion/Poly(vinyl alcohol-co-ethylene) Blends," *Smart Materials and Structures* 24, no. 10 (September 2015): 105011, <https://doi.org/10.1088/0964-1726/24/10/105011>.
45. V. Di Noto, R. Gliubbizzi, E. Negro, and G. Pace, "Effect of SiO₂ on Relaxation Phenomena and Mechanism of Ion Conductivity of [Nafion/(SiO₂)_x] Composite Membranes," *The Journal of Physical Chemistry B* 110, no. 49 (November 2006): 24972–24986, <https://doi.org/10.1021/jp0650331>.
46. D. G. Abebe and T. R. Farhat, "Self-Assembly of Nafion/Poly(vinyl alcohol) at pH = 1.2 and Nafion/Poly(allyl amine) at pH = 11," *Soft Matter* 6 (2010): 1325–1335, <https://doi.org/10.1039/b922653b>.
47. S.-Y. Choi, S. Cho, D. Kim, et al., "Boosting the Proton Conduction Using Protonated Imidazole for Advanced Ion Conducting Membrane," *Journal of Membrane Science* 620 (February 2021): 118904, <https://doi.org/10.1016/j.memsci.2020.118904>.
48. I. S. Amiinu, W. Li, G. Wang, et al., "Toward Anhydrous Proton Conductivity Based on Imidazole Functionalized Mesoporous Silica/Nafion Composite Membranes," *Electrochimica Acta* 160 (April 2015): 185–194, <https://doi.org/10.1016/j.electacta.2015.02.070>.
49. R. Sigwadi, M. S. Dhlamini, T. Mokrani, F. Némavhola, P. F. Nonjola, and P. F. Msomi, "The Proton Conductivity and Mechanical Properties of Nafion/ZRP Nanocomposite Membrane," *Heliyon* 5, no. 8 (August 2019): e02240, <https://doi.org/10.1016/j.heliyon.2019.e02240>.
50. H. Safardoust-Hojaghan, M. Salavati-Niasari, O. Amiri, and M. Hassanpour, "Preparation of Highly Luminescent Nitrogen Doped Graphene Quantum Dots and Their Application as a Probe for Detection of *Staphylococcus aureus* and *E. coli*," *Journal of Molecular Liquids* 241 (September 2017): 1114–1119, <https://doi.org/10.1016/j.molliq.2017.06.106>.
51. J. Wang, M. Musameh, and Y. Lin, "Solubilization of Carbon Nanotubes by Nafion Toward the Preparation of Amperometric Biosensors," *Journal of the American Chemical Society* 125, no. 9 (February 2003): 2408–2409, <https://doi.org/10.1021/ja028951v>.
52. S. Ansari, A. Kelarakis, L. Estevez, and E. P. Giannelis, "Oriented Arrays of Graphene in a Polymer Matrix by In Situ Reduction of Graphite Oxide Nanosheets," *Small* 6, no. 2 (January 2010): 205–209, <https://doi.org/10.1002/sml.200900765>.
53. V. Parthiban, S. K. Panda, and A. K. Sahu, "Highly Fluorescent Carbon Quantum Dots-Nafion as Proton Selective Hybrid Membrane for Direct Methanol Fuel Cells," *Electrochimica Acta* 292 (December 2018): 855–864, <https://doi.org/10.1016/j.electacta.2018.09.193>.
54. W. Jia, B. Tang, and P. Wu, "Carbon Dots With Multi-Functional Groups and the Application in Proton Exchange Membranes," *Electrochimica Acta* 260 (January 2018): 92–100, <https://doi.org/10.1016/j.electacta.2017.11.047>.

55. J. J. Richardson, M. Björnalm, and F. Caruso, "Technology-Driven Layer-by-Layer Assembly of Nanofilms," *Science* 348, no. 6233 (April 2015), <https://doi.org/10.1126/science.aaa2491>.
56. K. Schmidt-Rohr and Q. Chen, "Parallel Cylindrical Water Nanochannels in Nafion Fuel-Cell Membranes," *Nature Materials* 7, no. 1 (December 2007): 75–83, <https://doi.org/10.1038/nmat2074>.
57. L. Zhong, Y. Song, and S. Zhou, "The Effectiveness of Nafion-Coated Stainless Steel Surfaces for Inhibiting *Bacillus subtilis* Biofilm Formation," *Applied Sciences* 10, no. 14 (July 2020): 5001, <https://doi.org/10.3390/app10145001>.
58. V. D. Avvari and P. S. R. Sreekanth, "Performance of Teflon-Reinforced Nafion Against Microbes and Removal of Heavy Metal Ions From Aqueous Environment," *Results in Engineering* 22 (June 2024): 102253, <https://doi.org/10.1016/j.rineng.2024.102253>.
59. E. N. Gibbons, C. Winder, E. Barron, et al., "Layer by Layer Antimicrobial Coatings Based on Nafion, Lysozyme, and Chitosan," *Nanomaterials* 9, no. 11 (November 2019): 1563, <https://doi.org/10.3390/nano9111563>.
60. S. N. Riduan and Y. Zhang, "Imidazolium Salts and Their Polymeric Materials for Biological Applications," *Chemical Society Reviews* 42, no. 23 (2013): 9055, <https://doi.org/10.1039/c3cs60169b>.
61. S. Lee, H. Cheng, M. Chi, et al., "Sensing and Antibacterial Activity of Imidazolium-Based Conjugated Polydiacetylenes," *Biosensors and Bioelectronics* 77 (March 2016): 1016–1019, <https://doi.org/10.1016/j.bios.2015.10.090>.
62. R. A. Helmick, A. E. Fletcher, A. M. Gardner, et al., "Imidazole Antibiotics Inhibit the Nitric Oxide Dioxygenase Function of Microbial Flavohemoglobin," *Antimicrobial Agents and Chemotherapy* 49, no. 5 (May 2005): 1837–1843, <https://doi.org/10.1128/aac.49.5.1837-1843.2005>.
63. J. Liang, J. She, H. He, et al., "A New Approach to Fabricate Polyimidazolium Salt (PIMS) Coatings With Efficient Antifouling and Antibacterial Properties," *Applied Surface Science* 478 (June 2019): 770–778, <https://doi.org/10.1016/j.apsusc.2019.01.228>.
64. S. Karpagam and S. Guhanathan, "Phosphorus Based Indole and Imidazole Functionalized Hyperbranched Polyester as Antimicrobial Surface Coating Materials," *Progress in Organic Coatings* 77, no. 11 (November 2014): 1901–1910, <https://doi.org/10.1016/j.porgcoat.2014.06.022>.
65. W. Tian, H. Yang, H. Li, S. Wang, H. Jin, and L. Tian, "A Self-Healing Polyurethane/Imidazole-Modified Carboxylated Graphene Oxide Composite Coating for Antifouling and Anticorrosion Applications," *European Polymer Journal* 219 (October 2024): 113372, <https://doi.org/10.1016/j.eurpolymj.2024.113372>.
66. A. Biswas, P. Khandelwal, R. Das, et al., "Oxidant Mediated One-Step Complete Conversion of Multi-Walled Carbon Nanotubes to Graphene Quantum Dots and Their Bioactivity Against Mammalian and Bacterial Cells," *Journal of Materials Chemistry B* 5, no. 4 (2017): 785–796, <https://doi.org/10.1039/c6tb02446g>.
67. M. D. Rojas-Andrade, T. A. Nguyen, W. P. Mistler, et al., "Antimicrobial Activity of Graphene Oxide Quantum Dots: Impacts of Chemical Reduction," *Nanoscale Advances* 2, no. 3 (2020): 1074–1083, <https://doi.org/10.1039/c9na00698b>.
68. W.-S. Kuo, Y.-T. Shao, K.-S. Huang, T.-M. Chou, and C.-H. Yang, "Antimicrobial Amino-Functionalized Nitrogen-Doped Graphene Quantum Dots for Eliminating Multidrug-Resistant Species in Dual-Modality Photodynamic Therapy and Bioimaging Under Two-Photon Excitation," *ACS Applied Materials & Interfaces* 10, no. 17 (April 2018): 14438–14446, <https://doi.org/10.1021/acsami.8b01429>.
69. X. Zhang, S. Lu, D. He, et al., "Antibacterial Property of Graphene Quantum Dots-Modified TiO₂ Nanorods on Titanium Dental Implant," *Transactions of Nonferrous Metals Society of China* 33, no. 8 (August 2023): 2395–2405, [https://doi.org/10.1016/s1003-6326\(23\)66267-3](https://doi.org/10.1016/s1003-6326(23)66267-3).
70. M. S. Beg, E. N. Gibbons, S. Gavalas, M. A. Holden, M. Krysmann, and A. Kelarakis, "Antimicrobial Coatings Based on Amine-Terminated Graphene Oxide and Nafion With Remarkable Thermal Resistance," *Nanoscale Advances* 6, no. 10 (2024): 2594–2601, <https://doi.org/10.1039/d3na01154b>.
71. D. K. Paul and K. Karan, "Conductivity and Wettability Changes of Ultrathin Nafion Films Subjected to Thermal Annealing and Liquid Water Exposure," *The Journal of Physical Chemistry C* 118, no. 4 (January 2014): 1828–1835, <https://doi.org/10.1021/jp410510x>.
72. T. da S Pinto, L. A. Alves, G. de Azevedo Cardozo, et al., "Layer-by-Layer Self-Assembly for Carbon Dots/Chitosan-Based Multilayer: Morphology, Thickness and Molecular Interactions," *Materials Chemistry and Physics* 186 (January 2017): 81–89, <https://doi.org/10.1016/j.matchemphys.2016.10.032>.
73. X.-F. Zhang, L. Song, Z. Wang, Y. Wang, L. Wan, and J. Yao, "Highly Transparent Graphene Oxide/Cellulose Composite Film Bearing Ultraviolet Shielding Property," *International Journal of Biological Macromolecules* 145 (February 2020): 663–667, <https://doi.org/10.1016/j.ijbiomac.2019.12.241>.
74. C. Teng, X. Liu, M. Lin, and J. Li, "Flexible Graphene Oxide/Polyacrylonitrile Composite Films With Efficient Ultraviolet Shielding and High Transparency for the Protection of Paper-Based Artifacts," *Nordic Pulp & Paper Research Journal* 38, no. 1 (November 2022): 111–119, <https://doi.org/10.1515/npprj-2022-0074>.
75. S. Wongrekkdee and P. Pimpang, "Ultraviolet-Shielding and Water Resistance Properties of Graphene Quantum Dots/Polyvinyl Alcohol Composite-Based Film," *Journal of Metals, Materials and Minerals* 30, no. 4 (December 2020): 90–96, <https://doi.org/10.55713/jmmm.v30i4.722>.
76. N. Xu, S. Gao, C. Xu, Y. Fang, L. Xu, and W. Zhang, "Carbon Quantum Dots Derived From Waste Acorn Cups and Its Application as an Ultraviolet Absorbent for Polyvinyl Alcohol Film," *Applied Surface Science* 556 (August 2021): 149774, <https://doi.org/10.1016/j.apsusc.2021.149774>.
77. S. C. Hess, F. A. Permatasari, H. Fukazawa, et al., "Direct Synthesis of Carbon Quantum Dots in Aqueous Polymer Solution: One-Pot Reaction and Preparation of Transparent UV-Blocking Films," *Journal of Materials Chemistry A* 5, no. 10 (2017): 5187–5194, <https://doi.org/10.1039/c7ta00397h>.
78. M. Bakeshlouy Afshar, A. Poursattar Marjani, and P. Gozali Balkanloo, "Introducing Graphene Quantum Dots in Decomposable Wheat Starch-Gelatin Based Nano-Biofilms," *Scientific Reports* 14, no. 1 (January 2024), <https://doi.org/10.1038/s41598-024-52560-z>.

Supporting Information

Additional supporting information can be found online in the Supporting Information section.